J Eng Math (2018) 108:171–196
https://doi.org/10.1007/s10665-017-9918-6

Simulation of aerosol formation due to rapid cooling of multispecies vapors

Christoph Winkelmann · Arkadiusz K. Kuczaj · Markus Nordlund · Bernard J. Geurts

Received: 10 June 2015 / Accepted: 29 May 2017 / Published online: 29 June 2017

Abstract An extended classical nucleation approach is put forward with which aerosol formation from rapidly cooled, supersaturated multispecies vapor mixtures can be predicted. The basis for this extension lies in the treatment of the critical cluster that forms as part of the nucleation burst—a multispecies treatment of the thermodynamically consistent approach is proposed that can be solved efficiently with a Newton iteration. Quantitative agreement with Becker–Döring theory was established in case the equilibrium concentration of the critical clusters is properly normalized. The effects of nucleation, condensation, evaporation, and coalescence are consolidated in the numerical framework consisting of the Navier–Stokes equations with Euler–Euler one-way coupled vapor and liquid phases. We present a complete numerical framework concerning generation and transport of aerosols from oversaturated vapors and focus on numerical results for the aerosol formation. In particular, using adaptive time-stepping to capture the wide range of time scales that lie between the nucleation burst and the slower condensation and coalescence, the aerosol formation of a system of up to five alcohols in a carrier gas is studied. The effects of the temperature levels, the cooling rate, and the composition of the vapor mixture under a constant temperature drop, on the formation and properties of the aerosol are investigated. A striking nonuniform dependence of the asymptotic number concentration of aerosol droplets on temperature levels was found. A decrease of the rate of cooling was shown to reduce the number concentration of aerosol droplets which asymptotically leads to significantly larger droplets. The simplification of the vapor mixture by removing the higher alcohols from the system was found to yield an increase in the asymptotic size of the droplets of about 15%, while the number density was reduced accordingly.

C. Winkelmann · A. K. Kuczaj (✉) · M. Nordlund
Philip Morris International Research & Development, Philip Morris Products S.A. (part of Philip Morris International group of companies), Quai Jeanrenaud 5, 2000 Neuchâtel, Switzerland
e-mail: arkadiusz.kuczaj@pmi.com

Present address
C. Winkelmann
ABB Corporate Research Center, Power Device Simulations, Segelhofstrasse 1K, 5405 Baden-Dättwil, Switzerland

A. K. Kuczaj · B. J. Geurts
Multiscale Modeling & Simulation, Department of Applied Mathematics, University of Twente, P.O. Box 217, 7500 AE Enschede, The Netherlands
e-mail: b.j.geurts@utwente.nl

B. J. Geurts
Anisotropic Turbulence, Department of Applied Physics, Eindhoven University of Technology, P.O. Box 513, 5600 MB Eindhoven, The Netherlands

Keywords Aerosol · Alcohol mixtures · Evaporation and condensation · Multispecies · Nucleation

1 Introduction

The dynamics of an aerosol forming from a gaseous mixture of various chemical species is expressed by the detailed interplay between nucleation, evaporation, and condensation, as well as coalescence, interacting with vapor concentration, temperature, and velocity fields. We focus on an aerosol arising from nucleation in a supersaturated mixture of alcohol gases that is subjected to very rapid cooling. The prediction of the composition and size distribution of the droplets constituting the aerosol becomes particularly challenging when the number of species becomes large. The cornerstone approach in this field is the Becker–Döring (BD) theory [1], presenting a microscopic basis for the understanding of macroscopic properties of cluster formation in multispecies systems. However, in its full generality, this approach is unpractical for more than just a few species, requiring significant computational effort, even for steady-state cases, and the development of new solution methods [2] to reduce simulation costs. In this paper, we present and illustrate a modeling approach that is computationally much less demanding. It is based on an extension of classical nucleation theory, closely following [3,4], that allows approximating aerosol properties in multispecies systems. The new formulation can handle systems containing tens to hundreds of species, as is shown by determining the multispecies nucleation rate. This extends significantly the capability of classical aerosol modeling. The method will be illustrated for spatially homogeneous systems, for which a tailored adaptive time-stepping method is put forward to handle the very rapid nucleation burst, followed by the much slower evolution due to condensation and coalescence. We validate the new formulation by comparing full solutions of a ternary system of alcohol vapors based on the numerical solution to the BD equations [5]. The capability of the new approach is illustrated by studying aerosols from alcohol vapors containing up to five different species, for which the size distribution of the aerosol droplets as well as the chemical composition is computed under different initial temperatures and cooling rates at constant pressure drop.

Classical nucleation theory concentrates on the prediction of the so-called 'critical cluster.' This term designates a grouping of molecules from the gas phase that is large enough to stay coherent for long times with probability of one half. It signifies the 'border' of transient molecular aggregates; on average, smaller clusters are likely to disintegrate rather quickly into the gas phase, while larger clusters would likely grow on average. The critical cluster is identified as the key nucleation core from which droplets would grow due to condensation of molecules from the vapor. Virgin droplets that just nucleated are treated as if emerging with a certain start-up diameter. Subsequently, the size can grow by several orders of magnitude, e.g., due to rapid cooling of the surrounding vapor inducing condensation. In this process the composition of the droplets also changes in accordance with the molar volume of the components and their saturation. This basic physical setting is presented in this paper, extending the ternary formulation presented in [3,4] to an arbitrary number of components. The formulation requires a fast determination of the properties of the critical cluster in order to start up the aerosol evolution. This problem will be addressed in this paper.

A recent study based on Becker–Döring theory was presented in [5], considering the mixtures of alcohols in particular. A specialized multigrid solver was developed in order to efficiently solve the composition of droplets in n-component mixtures. The method was illustrated for up to five alcohols simultaneously, which constitutes the state of the art for a computational approach based on the Becker–Döring approach. Here, we do not follow the Becker–Döring methodology but rather consider a simpler theory, generalizing earlier work by Wilemski [4], in which multispecies nucleation is treated including the interaction between the species. This approach can be used for situations in which one of the components is dominant [6], but also for more complex nucleation problems with several components taking part in the nucleation process. The composition of the critical cluster can be determined on the basis of finding the root of the equation governing the molar fractions. Newton iteration was used to efficiently solve the molar fractions problem, solving the problem with little computational overhead for many components. We present the theory and illustrate the critical cluster properties for a number of characteristic situations.

An important challenge for classical nucleation approaches of multispecies systems is the validation against well-controlled physical experiments. A prominent example is the laminar flow diffusion chamber (LFDC) in which an aerosol is formed due to rapid cooling under slow flow conditions. This requires the treatment of (a) the multispecies aerosol formation and (b) the capturing of spatial variations and details of the geometry of the experimental equipment. In this paper, we address the first element and focus on spatially homogeneous systems in which aerosol forms from a supersaturated vapor mixture, obtained by very rapid external cooling. The element of simultaneous laminar fluid flow will be integrated in later studies and is a subject of ongoing research. To allow at this stage a cross-validation with fully resolved Becker–Döring theory [5], the method is illustrated for a system of alcohol vapors. Effects of (a) the temperature levels, (b) the cooling rate, and (c) the mixture composition will be investigated, and the consequences for the droplet composition and sizes are determined using the new model. Compared to full Becker–Döring theory, the approximate model is computationally inexpensive and applicable to large numbers of species.

The intention of this paper is two-fold. First, we will provide a complete computational framework for multispecies aerosol including its formation, evolution, and transport taking into account all explicitly stated assumptions. Subsequently, the second part of this paper delivers detailed insight into the algorithm and accuracy of the presented nucleation model in a spatially homogeneous formulation. Further investigations that include spatially inhomogeneous transport for the coupled conservation equations are subject of ongoing research (see [7]). The organization of the paper is as follows. In Sect. 2, an extended model for nucleation of droplets from a supercritical vapor mixture and their subsequent evolution due to evaporation and condensation is presented, capable of treating systems with many chemical species. The formation of the critical clusters is at the root of the nucleation process and an algorithm for their chemical composition is discussed in Sect. 3, next to a method for efficient adaptive time-stepping. The dynamics of the aerosol that emerges from a mixture of alcohol vapors is simulated under various cooling conditions and presented in Sect. 4. Concluding remarks are contained in Sect. 5.

2 Extended classical nucleation theory for many species mixtures

In this section, we present a general framework for multispecies aerosol formation and evolution, applicable to large numbers of species at low computational effort. First, we introduce the transport equations in Sect. 2.1, following the conventional ‘Euler–Euler’ setting. The source terms describing nucleation, condensation, and evaporation, as well as coalescence of the aerosol will be presented in Sects. 2.2, 2.3, and 2.4. In order to develop this model, the single-species aerosol formation was studied in detail in [6] standing as a base for further multispecies model extensions. Multispecies representation requires the re-definition of the aerosol formation (nucleation) model, in which a novel approach for the critical cluster composition and condensation rate was introduced. This applies also for the other submodels, e.g., the condensation/evaporation model must also take into account the multispecies character of the gas/liquid mixtures. The framework presented in this section serves as a complete source of information to build an Eulerian two-moment multispecies aerosol physics approach coupled with the computational fluid dynamics equations represented by the conservation laws. Furthermore, thermo-physical properties of several basic acyclic alcohols, composing the aerosol formers for the nucleation model system studied in this paper, are discussed in Sect. 2.5. The dynamic system that governs the evolution of the aerosol in a spatially homogeneous system is summarized in Sect. 2.6.

2.1 Multispecies aerosol transport equations including phase transition

In this section, we formulate a general system of multiphase transport equations describing the evolution of a multispecies aerosol. We consider the total system to be composed of dispersed droplets, next to a mixture of carrier gas (e.g., air) and vapors that constitute the transporting medium and the source of chemical components, respectively. We adopt an Euler–Euler formulation in which the gaseous ‘carrier phase’, i.e., carrier gas and aerosol-

forming vapors, and the aerosol droplets are represented by continuous fields. We assume that the droplets are sufficiently small in order to precisely follow the flow, i.e., the relative velocity with respect to the carrier phase can be neglected. Likewise, the droplets are assumed to have immediate heat transfer with the carrier phase such that the temperature of all phases may be treated as being the same.

The dynamics of a general multispecies aerosol can be formulated by incorporating conservation laws for mass, momentum, enthalpy, gaseous, and liquid mass fractions of the various constituents and the droplet number concentrations. Extending the formulation by Winkelmann et al. [6] to the general multispecies case, we may write the dominant processes as

$$\begin{aligned}
\partial_t \rho + \partial_j(\rho u_j) &= 0,\\
\partial_t(\rho u_i) + \partial_j(\rho u_i u_j) &= -\partial_i p + \partial_j(\mu\tau_{ij}); \quad i = 1,\ldots,3,\\
\rho c_p(\partial_t T + u_j\partial_j T) &= \partial_j(K\partial_j T) + \partial_j(\mu u_k\tau_{kj}) + S_h + \frac{Dp}{Dt},\\
\partial_t(\rho Y_i) + \partial_j(\rho Y_i u_j) &= \partial_j(\rho D_i\partial_j(Y_i)) + S_i^{l\to v}; \quad i = 1,\ldots,n,\\
\partial_t(\rho Z_i) + \partial_j(\rho Z_i u_j) &= -S_i^{l\to v},\\
\partial_t(N) + \partial_j(N u_j) &= S_{\mathrm{N}},
\end{aligned} \tag{1}$$

where ∂_t and ∂_j denote partial differentiation with respect to time t and spatial coordinate x_j, respectively, and summation over j and k is implied, while no summation over i is adopted. The total mass density of the n-species system is denoted by ρ, while the velocity and temperature fields of the carrier phase are given by u_i and T, respectively. The material derivative of the pressure Dp/Dt contributes directly to the changes in the local temperature. The heat capacity at constant pressure is denoted by c_p and approximated as a function of temperature alone, implying that the system studied in this paper is mainly composed of carrier gas containing a relatively small fraction of aerosol-forming vapors. For improved solution accuracy, all material properties (e.g., heat capacity, viscosity, heat conductivity) should follow adequate mixture laws that for example can be found in [8].

Mass fraction equations for $\{Y_i, Z_i\}$ in (1) describe the partitioning between gaseous and liquid aerosol phases containing mass transfer source terms that will be introduced momentarily. The particle number density equation for N gives further information concerning the characterization of the aerosol. Mass fraction equations must be consistent with the global mass conservation equation that specifies the overall density of the considered mixture. At the same time, the particle number density equation must be consistent with the liquid mass fraction equations to account for the aerosol transport in the system. We assume a fixed log-normal aerosol size distribution in the system, as is commonly done in moment equation models. Transport of liquid mass fractions together with the evolving particle number density provides information about the average aerosol droplet size. This may vary depending on the mass transfer (condensation/evaporation) and transport (convection and coalescence) processes in the system. Nucleation of aerosol affects both mass and particle number density. The assumed log-normal distribution excludes a closer connection to possible multi-modal corrections as observed in some model studies [9]. In this paper, we focus on the accuracy of model predictions as governed by the temporal integration method, resolving very fast nucleation scales as well as much slower condensation and evaporation. The same log-normal approach implies that aerosol polydispersity will only influence the average diameter of the droplets and not the fluctuations. Finally, we assume a homogeneous temperature equilibration between the phases in which effects of phase changes are represented by the enthalpy of vaporization. More involved formulations that assign different temperatures to the gas phase and the liquid phase are not pursued here.

Soret and Dufour effects were discarded for the present studies. The rate of strain tensor is given by

$$\tau_{ij} = \partial_i u_j + \partial_j u_i - \frac{2}{3}\partial_k u_k \delta_{ij}, \tag{2}$$

where δ_{ij} denotes the Kronecker delta. We also introduced the heat conductivity K to characterize the diffusive transport of heat.

The multispecies aerosol is characterized in terms of the mass fractions of the components i in the gas phase (Y_i) and in the droplet phase (Z_i). These mass fractions are such that ρY_i and ρZ_i yield the partial densities of component i in the gas and droplet phase, respectively. For a system with n species, either in vapor or in liquid form, these fractions fulfill the following constraint:

$$\sum_{i=1}^{n}(Y_i + Z_i) = 1. \tag{3}$$

This property is guaranteed by the sum of mass conservation equations for each species. Special numerical care must be taken concerning the consistency of those equations with the total mass conservation as the full system of Eq. (1) is mathematically over-constrained in this representation.

We also introduced diffusive transport of the vapor of species i through Fick diffusion with binary diffusion coefficients D_i of species i in the carrier gas. The values of these diffusion coefficients can be computed following [10,11]. We adopt Fuller's method [12] to approximate the coefficients for diffusive transport of a vapor of alcohol species i in a surrounding consisting mainly of carrier gas. We return to this momentarily in Sect. 2.5. The system pressure may be expressed as

$$p = \sum_{i=1}^{n} p_i^v; \quad p_i^v = \rho k T \frac{Y_i}{m_i}, \tag{4}$$

in terms of the partial vapor pressures p_i^v of the components i. These can be computed using Dalton's law and the ideal gas law in case the volume fraction of the droplets is sufficiently small. Here k denotes Boltzmann's constant and m_i is the molecular mass of species i, i.e., the mass of one molecule of species i. Diffusion of liquid droplets is not included because the diffusion coefficient of droplets is orders of magnitude smaller than that of the corresponding vapor. In addition, we track the number concentration of the droplets, N, allowing to assess also information about the size of the aerosol droplets.

To complete the basic model (1) three source terms need to be specified:

(i) Mass transfer between the liquid and the vapor of species i, denoted by $S_i^{l\to v}$. This contains two contributions: the nucleation mass flow rate S_i^{nuc}, characterizing vapor changing into liquid, and the mass flow rate due to evaporation of vapor from already formed droplets minus that due to condensation onto these droplets, $S_i^{\mathrm{e-c}}$, such that

$$S_i^{l\to v} = -S_i^{\mathrm{nuc}} + S_i^{\mathrm{e-c}}. \tag{5}$$

(ii) The heat flow rate due to phase change, denoted by S_{h}. This can be computed by summing the products of $S_i^{l\to v}$ of species i with the heat of evaporation of that species $\Delta h_i^{\mathrm{vap}}$:

$$S_{\mathrm{h}} = -\sum_{i=1}^{n} \Delta h_i^{\mathrm{vap}} S_i^{l\to v}. \tag{6}$$

(iii) The rate of change of the number concentration of droplets

$$S_{\mathrm{N}} = J_{\mathrm{N}} - J_{\mathrm{c}} - J_{\mathrm{ev}}, \tag{7}$$

in which we distinguish the nucleation rate J_{N}, the coalescence rate J_{c}, and the rate of complete droplet evaporation J_{ev}. Complete evaporation in an Eulerian aerosol model is a subject in its own right. In this paper, we will not address this issue and concentrate on situations in which droplets, once formed, undergo

size changes through condensation and evaporation, but are assumed to never fully disappear because of evaporation. This assumption is well satisfied, e.g., in situations in which only cooling of a freshly nucleated aerosol would take place, a process dominated by condensation. We consider $J_{\mathrm{ev}} = 0$ in this paper. Coalescence is often negligible during fast nucleation bursts. It does play a role in the much slower dynamics of aerosol evolution on longer time scales. In this paper, we include a simple model for J_{c} as specified in Sect. 2.4.

In the next three sections, we will specify the various source terms and include nucleation, evaporation and condensation, and coalescence, respectively.

2.2 Nucleation of aerosol

In this section, we present a generalization of classical multi-component theory for homogeneous nucleation, starting from work on ternary nucleation by Arstila et al. [3]. This theory is applicable both to situations in which one of the components is dominant in super saturation as well as to situations in which a number of species engage in the nucleation simultaneously. In situations where only one component dominates in saturation, one might also adopt homogeneous nucleation theory for that species [6] to a good approximation. The more complete situation in which several species contribute to the nucleation process requires that one accounts for the coupling between the nucleating species as well, e.g., expressed by 'competition' for energy. For example, energy that is released by the nucleation of a particular species, will affect the local temperature and thereby the nucleation rates of other species as well. It is not easy to determine whether one component is dominant in saturation or not. In fact, two components with very different partial vapor pressures and very different saturation vapor pressures can have similar saturations (also called 'activities' in some literature [5] in case a mixture of species is concerned). Therefore, a general classical multispecies nucleation theory is formulated here.

The specification of the nucleation rate J_{N} and the corresponding nucleation mass flow rates of the species S_i^{nuc} is presented in four steps. These are specified next.

1. The first element in the nucleation model concerns the formation of the virgin core from which aerosol droplets will form later. The composition of the so-called 'critical cluster' is described next, i.e., the cluster whose size is such that it has an equal probability to subsequently grow or shrink due to evaporation and condensation to and from the surrounding vapors. For that purpose, we introduce [4] the actual vapor pressure of species i, denoted by p_i, and the corresponding saturation vapor pressure of species i in the current mixture, $p_{i,\mathrm{sat}}^{\mathrm{mix}}$. In addition, we denote the partial molar volume by v_i. Formally extending the thermodynamically consistent classical nucleation theory [3] to an arbitrary number of species suggests that the composition of the critical cluster is such that

$$f_1 = f_2 = f_3 = \cdots = f_n, \quad \text{where} \quad f_i = \frac{1}{v_i} \ln\left(\frac{p_i}{p_{i,\mathrm{sat}}^{\mathrm{mix}}}\right). \tag{8}$$

The commonly used saturation pressure of the pure component i, which arises above a surface of the pure liquid of that component held at temperature T, denoted by p_i^{sat}, can now be used to define the saturation of species i, i.e., $S_i \geq 0$, and the mole fraction of species i in the critical cluster, i.e., $0 \leq w_i \leq 1$ as

$$p_i = S_i\, p_i^{\mathrm{sat}}; \quad p_{i,\mathrm{sat}}^{\mathrm{mix}} = w_i\, p_i^{\mathrm{sat}}. \tag{9}$$

This relation applies if Raoult's law holds [11]. With these definitions we may express the conditions from which the composition of the critical cluster in the n-component mixture can be obtained as

$$f_i = \frac{1}{v_i} \ln\left(\frac{S_i}{w_i}\right) = \alpha; \quad i = 1, 2, \ldots, n, \tag{10}$$

where α is *a priori* unknown and specified by the auxiliary condition that

$$\sum_{i=1}^{n} w_i = 1; \quad w_i \geq 0. \tag{11}$$

Combined, the system of equations (10) and (11) constitute $n + 1$ equations for the $n + 1$ unknowns $\{\alpha, w_1, \ldots, w_n\}$. The mole fractions in the critical cluster can be obtained once the saturations of all species S_i and their partial molar volumes v_i are specified. We may extract the mole fraction of species i from (10) as

$$w_i = S_i \exp(-\alpha v_i). \tag{12}$$

Since we require the solution to be also a partition of unity, we obtain a consistency relation for α:

$$f(\alpha) = \left(\sum_{i=1}^{n} S_i \exp(-\alpha v_i) \right) - 1 = 0. \tag{13}$$

This is also referred to as the mole fraction equation. We may solve this problem for α iteratively as shown and analyzed in Sect. 3 in which we also consider the dependence of the composition on the saturation and the partial molar volume.

2. The second step in the determination of the nucleation rate is the calculation of the equilibrium concentration of critical clusters, denoted by c_{eq}. We adopt an ideal mixture approximation in which the surface tension σ of the critical cluster may be written as

$$\sigma = \sum_{i=1}^{n} w_i \sigma_i, \tag{14}$$

in which σ_i denotes the surface tension of component i. These quantities depend on temperature, for which accurate approximations are available in literature for a wide range of components [13]. The specification of the thermo-physical properties of a range of the smaller acyclic alcohols is postponed until Sect. 2.5. The radius of the critical cluster r can be calculated from [3]

$$r = \frac{2\sigma v}{kT \sum_{i=1}^{n} w_i \ln(S_i/w_i)} = \frac{2\sigma}{kT\alpha}, \tag{15}$$

in which we introduced the average molecular volume v through an ideal mixture law $v \equiv \sum_{i=1}^{n} w_i v_i$.
After these preparations, the Gibbs free energy barrier ΔG of the critical cluster, measuring the energy needed for the formation of a critical cluster with radius r and a surface tension σ, can be expressed as

$$\Delta G = \frac{4}{3}\pi r^2 \sigma. \tag{16}$$

This allows calculating the equilibrium concentration c_{eq} of critical clusters. In fact, from statistical mechanics, $c_{\text{eq}} \sim \exp(-\Delta G/kT)$ with normalization still to be specified. The correct normalization is subject of much discussion in literature [14]. We consider two options for completing the expression for c_{eq}. A crude approximation, based on the partial vapor pressures of the species involved in the nucleation can be written as

$$c_{\text{eq}} = \exp\left(-\frac{\Delta G}{kT}\right) \sum_{i=1}^{n} \frac{H(w_i) p_i^v}{kT}, \tag{17}$$

where H denotes Heaviside's function $H(z) = 1$ if $z > 0$ and 0 otherwise. In this expression only the species actually contained in the critical cluster, i.e., with $w_i > 0$, contribute a factor p_i^v/kT and the total represents a sum over monomer concentrations [3]. This normalization is know to be physically inconsistent in some limiting cases [5]. A refinement for the determination of the equilibrium concentration c_{eq} is obtained by adopting a so-called 'self-consistent' normalization [14], which is mathematically consistent in the limits of single-species conditions [2]. In fact, introducing the single species, or 'monomer,' surface area

$$s_i^{\mathrm{mon}} = (36\pi)^{1/3} v_i^{2/3}, \tag{18}$$

the equilibrium concentration is expressed as

$$c_{\mathrm{eq}} = \exp\left(-\frac{\Delta G}{kT}\right) \prod_{i=1}^{n} \left(\frac{p_i^{\mathrm{sat}}(T)}{kT} \exp\left(\frac{s_i^{\mathrm{mon}} \sigma_i}{kT}\right)\right)^{w_i}, \tag{19}$$

in terms of the species saturation pressure p_i^{sat}.

3. The third step leading toward the completion of the nucleation rate is the specification of the Zeldovich factor, which characterizes the contribution of Brownian motion to the formation of the critical cluster [15]. As proposed in [3] this factor can be approximated as

$$Z = \left(\frac{\sigma v^2}{kT 4\pi^2 r^4}\right)^{1-n_{\mathrm{nuc}}/2}, \tag{20}$$

in terms of the number of components that is actually involved in the nucleation, n_{nuc}. The latter can conveniently be expressed as

$$n_{\mathrm{nuc}} = \sum_{i=1}^{n} H(w_i). \tag{21}$$

4. The fourth and final preparation step toward an expression for the nucleation rate concerns the determination of the average growth rate. The total number of molecules in the critical cluster can be expressed as $N_{\mathrm{tot}} = (4/3)\pi r^3/v$, which allows to compute the number of molecules of component i in such a cluster as $N_i = N_{\mathrm{tot}} w_i$, and the total mass of the cluster as $m = \sum_{i=1}^{n} N_i m_i$. Under the assumption that cluster–cluster collisions can be neglected, i.e., in the sufficiently dilute state, the condensation rate K_{ii} of component i can be found from [3]

$$K_{ii} = \left(\frac{p_i^v}{kT}\right)\left(\frac{3}{4\pi}\right)^{1/6} (6kT)^{1/2} \left(\frac{1}{m_i} + \frac{1}{m}\right)^{1/2} \left(\left(\frac{m_i}{\rho_i^1}\right)^{1/3} + \left(\frac{4\pi}{3}\right)^{1/3} r\right)^2. \tag{22}$$

Extending the ternary expression for the average growth rate R_{av} as proposed in [3] to a general system of n components, we formally arrive at

$$R_{\mathrm{av}} = \frac{\sum_{i=1}^{n} N_i^2}{\sum_{i=1}^{n} N_i^2/K_{ii}} = \frac{\sum_{i=1}^{n} w_i^2}{\sum_{i=1}^{n} w_i^2/K_{ii}}. \tag{23}$$

After these four preparatory steps, we may summarize the nucleation rate J_N as

$$J_N = R_{av} Z c_{eq}. \tag{24}$$

The nucleation mass flow S_i^{nuc} for component i can be written as

$$S_i^{nuc} = 2 J_N N_i m_i, \tag{25}$$

where the freshly nucleated droplet is given a mass equal to twice that of the critical cluster, thereby expressing that these virgin droplets are likely to grow after nucleation, while the critical clusters are by definition such that they have equal probability to grow or shrink after nucleation.

The expression for the nucleation rate J_N is typical for currently adopted classical nucleation theory in the sense that it rests largely on phenomenological physics and scaling arguments clarifying the main dependencies and mechanisms and capturing the expected order of magnitudes. In all this, the normalization of the equilibrium concentration c_{eq} is very important to the final level of quantitative agreement with physical reality that is achieved. A key point of reference for gaging the phenomenological expression for J_N is the seminal Becker–Döring theory [1,16], which constitutes a fundamental microscopic treatment of the nucleation process. It is computationally rather expensive for systems with many species but in some cases the n-component Becker–Döring equations can be solved in full detail [2], thereby allowing to cross-validate the developed model for the nucleation rate J_N with the full numerical solution. We return to this cross-validation and motivation of the appropriate normalization of c_{eq} in Sect. 3.1.

2.3 Evolution of aerosol by evaporation and condensation

Evaporation and condensation are two sides of one mechanism—that of gas–liquid mass transfer. While evaporation relates to net mass transfer from the liquid droplets to the gas phase, condensation is net mass transfer from the gas phase to the droplet phase. Evaporation (or condensation) will make the droplets shrink (or grow), but it will not change the number of droplets. For multispecies evaporation and condensation in the dilute regime, as considered here, one may treat all components independently as proposed by Friedlander [17], Wilck and Stratmann [18]. A more elaborate treatment including full coupling between the various species as proposed in [19] is not used here.

In order to derive an expression for the evaporation and condensation mass flow rate S_i^{e-c} of component i, we need to collect expressions of a number of constituting factors. The desired mass flow rate is proportional to the number density of droplets N and should be sensitive to whether the saturation is larger or smaller than the equilibrium saturation. In addition, specific transport properties such as diffusion should be incorporated to quantify S_i^{e-c}. We specify the various elements next.

We may characterize the droplet phase by its overall density

$$\rho_l = \frac{\sum_{i=1}^{n} Z_i}{\sum_{i=1}^{n} Z_i / \rho_i^l}, \tag{26}$$

in terms of the mass density of the liquid of component i denoted by ρ_i^l. On this basis, we may compute the so-called diameter of average mass d_m of the polydisperse aerosol

$$d_m = \left(\frac{6\rho \sum_{i=1}^{n} Z_i}{\pi \rho_l N} \right)^{1/3} = \left(\frac{6\rho \sum_{i=1}^{n} Z_i / \rho_i^l}{\pi N} \right)^{1/3}. \tag{27}$$

For computing the evaporation and condensation rate, the 'count mean diameter' $\overline{d}$ is required. Assuming a log-normal distribution of the droplet size with geometric standard deviation s_g we may relate $\overline{d}$ to d_m through the

Hatch–Choate conversion equation [20]:

$$\overline{d} = d_{\mathrm{m}} \exp\Big(- \ln^2(s_{\mathrm{g}})\Big). \tag{28}$$

The equilibrium saturation of component E_i is not equal to unity in view of the Kelvin effect. In fact, as given by [18]

$$E_i = \exp\left(\frac{4\sigma v_i}{kT\overline{d}}\right), \tag{29}$$

where the surface tension of the composite droplet is taken as

$$\sigma = \sum_{i=1}^{n} W_i \sigma_i, \tag{30}$$

expressed using the surface tension of droplets σ_i of pure component i and the mole fraction in the droplet's phase

$$W_i = \frac{Z_i/m_i}{\sum_{j=1}^{n} Z_j/m_j}, \tag{31}$$

where m_j denotes the molecular mass of component j. The saturation mole fraction X_i^{s} of component i in the gas phase over the droplets can be obtained from Raoult's law as

$$X_i^{\mathrm{s}} = W_i \frac{p_i^{\mathrm{s}}(T)}{p}, \tag{32}$$

where for the saturation pressure $p_i^{\mathrm{s}}(T)$ an appropriate empirical law is assumed. The corresponding saturation mass fraction Y_i^{s} can now be computed as

$$Y_i^{\mathrm{s}} = \frac{X_i^{\mathrm{s}} m_i}{X_i^{\mathrm{s}} m_i + (1 - X_i^{\mathrm{s}}) m_{\mathrm{g}}}, \tag{33}$$

with the average molecular mass of the gas phase given by

$$m_{\mathrm{g}} = \frac{\sum_{i=1}^{n} Y_i}{\sum_{i=1}^{n} Y_i/m_i}. \tag{34}$$

To complete the phenomenological theory for the mass flow rate $S_i^{\mathrm{e-c}}$ it is common to introduce the Fuchs factor f, also called Knudsen correction [20], which may be written as

$$f = \frac{1 + 2(\lambda/\overline{d})}{1 + 5.33(\lambda/\overline{d})^2 + 3.42(\lambda/\overline{d})}, \tag{35}$$

in terms of the mean free path λ given by

$$\lambda = \left(\frac{8kT}{\pi m_{\mathrm{g}}}\right)^{1/2} \left(\frac{4\mu}{5p}\right). \tag{36}$$

The final shape for the mass flow rate due to evaporation and condensation is expressed as

$$S_i^{\mathrm{e-c}} = 2\pi D_i \overline{d} \rho Y_i^{\mathrm{s}} f(\overline{d}, \lambda) \left(E_i - \frac{S_i}{W_i} \right) N. \tag{37}$$

This expression contains evaporation provided $E_i - S_i/W_i > 0$ and condensation if $E_i - S_i/W_i < 0$, and it is proportional to the number concentration of droplet N as anticipated earlier when starting the specification of $S_i^{\mathrm{e-c}}$. The saturation mass fraction Y_i^{s} is approximated by its value over a flat surface, as suggested by [18], while a 'Kelvin correction' accounting for the curvature of aerosol droplet surfaces is included through $(E_i - S_i/W_i)$. Such a Kelvin correction might also be motivated for the evaluation of Y_i^{s} itself by selecting

$$X_i^{\mathrm{s}} = W_i E_i \frac{p_i^{\mathrm{s}}(T)}{p}. \tag{38}$$

This proposal would, however, not correspond to the original suggestion of [18] and will not be incorporated here. Additional simulations based on such 'double Kelvin correction' showed largely similar results with, e.g., up to about 10% lower values for N for the cases considered.

2.4 Coalescence effects in aerosol dynamics

The coalescence rate J_{c} of droplets can be calculated based on the theory for polydisperse aerosols as put forward in [21]. First, the coalescence coefficients for the asymptotic regimes of large droplets, K_{l}, and of small droplets K_{s} are required. In the large droplets regime, the coalescence coefficient is approximated by

$$K_{\mathrm{l}} = \frac{2kT}{3\mu} \left(1 + \exp\left(\ln^2(s_{\mathrm{g}}) \right) + \frac{2.49\lambda}{d_{\mathrm{m}}} \left[\exp\left(2\ln^2(s_{\mathrm{g}}) \right) + \exp\left(4\ln^2(s_{\mathrm{g}}) \right) \right] \right), \tag{39}$$

while in the small droplets regime we adopt

$$K_{\mathrm{s}} = \sqrt{\frac{3kT d_{\mathrm{m}}}{\rho_{\mathrm{l}}}} \left(1 + \frac{1}{s_{\mathrm{g}}} \right)^{-1/2} \left[\exp\left(\frac{19}{8} \ln^2(s_{\mathrm{g}}) \right) + 2\exp\left(-\frac{1}{8} \ln^2(s_{\mathrm{g}}) \right) + \exp\left(-\frac{5}{8} \ln^2(s_{\mathrm{g}}) \right) \right]. \tag{40}$$

These two regimes are crudely combined into an effective coalescence coefficient $\overline{K}$ by averaging in the following way

$$\overline{K} = \left(K_{\mathrm{l}}^{-2} + K_{\mathrm{s}}^{-2} \right)^{-1/2}. \tag{41}$$

The coalescence rate J_{c} may then be computed as

$$J_{\mathrm{c}} = \overline{K} N^2. \tag{42}$$

This expression approximates the coalescence process in a simplified manner and mainly expresses proportionality with N^2, motivated by binary collisions as dominant coalescence mechanism. We will mainly be concerned with systems for which coalescence is a rather small effect, which implies that it mainly influences the long-term evolution of N, while being less important during the rapid burst of nucleation and subsequent condensation that characterizes a virgin aerosol.

Table 1 Parameters defining thermo-physical properties of the several acyclic alcohols $C_iH_{2i+1}OH$ considered in this paper: ethanol ($i = 2$), propanol ($i = 3$), butanol ($i = 4$), pentanol ($i = 5$), and hexanol ($i = 6$)

i	$\frac{p_{c,i}}{10^6}$	α_i	β_i	γ_i	δ_i	$T_{c,i}$	A_i	B_i	$10^3 a_i$	$10^3 b_i$
2	6.13	−8.69	1.18	−4.88	−1.59	513.92	1060.6	0.96	24.05	0.083
3	5.17	−8.54	1.96	−7.69	−2.95	536.78	1050.1	0.85	25.26	0.078
4	4.42	−8.41	2.23	−8.25	−0.71	563.05	1050.3	0.88	27.18	0.090
5	3.91	−8.98	3.92	−9.91	−2.19	588.15	1049.8	0.79	27.54	0.087
6	3.47	−9.49	5.13	−10.58	−5.15	610.70	1044.1	0.77	26.44	0.087

The parameters are represented in terms of Pa ($p_{c,i}$), K ($T_{c,i}$), $kg\,m^{-3}$ (A_i), $kg\,m^{-3}K^{-1}$ (B_i), Nm^{-1} (a_i), and $Nm^{-1}K^{-1}$ (b_i)

2.5 Thermo-physical properties of acyclic alcohols

In order to achieve an accurate representation of the aerosol dynamics of an alcohol mixture, the thermo-physical properties of the individual species need to be specified. In particular, the temperature dependence of the saturation pressure p_s, the liquid density ρ_l, and the surface tension σ need to be specified. In addition, the molecular mass m_i and the diffusion characteristics of the species in carrier gas are required. Closely following [5], we express $(p_{s,i}, \rho_{l,i}, \sigma_i)$ for $i = 2, \ldots, n$ as

$$p_{s,i}(T) = p_{c,i} \exp\left(\frac{\alpha_i \tau_i + \beta_i \tau_i^{3/2} + \gamma_i \tau_i^{5/2} + \delta_i \tau_i^5}{T_{r,i}}\right), \tag{43}$$

$$\rho_{l,i}(T) = A_i - B_i T, \tag{44}$$

$$\sigma_i(T) = a_i - b_i(T - T_{ref}), \tag{45}$$

where we introduced for each species i the following variables: (i) species-specific pressure $p_{c,i}$, (ii) $\tau_i = 1 - T_{r,i}$, with (iii) reduced temperature $T_{r,i} = T/T_{c,i}$ in terms of the species-specific temperature $T_{c,i}$. This phenomenological description is characterized by 10 parameters for each of the species, i.e., $(p_{c,i}, \alpha_i, \beta_i, \gamma_i, \delta_i, T_{c,i}, A_i, B_i, a_i, b_i)$, and a reference temperature taken here as $T_{ref} = 273.15$ K. The parameters are collected in Table 1. The $i = 1$ species represents the dominant carrier gas component (Argon in this paper).

To complete the specification of the material parameters, the molecular masses and the diffusion coefficients are required. The molecular weights are found from the molar weight, divided by Avogadro's number. For the molar weights M_i we collected (in kg): 0.04607, 0.06009, 0.07412, 0.08815, and 0.1022 for ethanol, propanol, butanol, pentanol, and hexanol. For the diffusion coefficients D_i of species i diffusing in carrier gas, we use Fuller's method. In fact, binary diffusion of species i in carrier gas at temperature T and pressure p is approximated by

$$D_i = 1.013 \times 10^{-2} \left(\frac{T^{1.75}}{p}\right) \frac{\left[M_{cg}^{-1} + M_i^{-1}\right]^{1/2}}{\left((V_{cg}^{diff})^{1/3} + (V_i^{diff})^{1/3}\right)^2}, \tag{46}$$

where M_{cg} and M_i denote the molar weights of N_A molecules of carrier gas and species i, and the so-called diffusion volume for carrier gas V_{cg}^{diff} is taken as that of Argon, i.e., 16.2. For the diffusion volumes of the various alcohol species, we adopt Fuller's method which takes the chemical formulae of the species and for every atom in the formula uses a contributing factor. For the acyclic alcohols we have as formula $C_iH_{2i+1}OH$, which leads to

$$V_i^{diff} = Ai + B(2i + 2) + C, \tag{47}$$

with $A = 15.9$, $B = 2.31$, and $C = 6.11$ denoting the molecular diffusion volumes for C, H, and O, respectively. Fuller's method of approximating the binary diffusion coefficient is estimated to yield not more than 4% error

[22], which appears suitable for the current dilute system. A more complete solution involving the Maxwell–Stefan diffusion formalism for the diffusion coefficients is not pursued here (see [23] and references therein).

2.6 Dynamic model for multispecies aerosol evolution

In order to study the effects of nucleation and evolution through evaporation and condensation of a mixture of alcohols, we consider a spatially homogeneous system. The simplified model with which nucleation bursts can be studied is extracted from (1) by formally setting the transporting velocity equal to zero and taking the mass density ρ constant. Moreover, instead of solving the evolution equation for the temperature, we externally impose a time-dependent T to represent cooling of a supercritical vapor mixture in carrier gas. The remaining system of ordinary differential equations governs the mass fractions of gas and liquid Y_i and Z_i, and the number concentration N. This yields a system of $2n + 1$ differential equations for (Y_i, Z_i, N) given by

$$\frac{\mathrm{d}Y_i}{\mathrm{d}t} = \rho^{-1} S_i^{l\to v}; \quad \frac{\mathrm{d}Z_i}{\mathrm{d}t} = -\rho^{-1} S_i^{\mathrm{l}\to v}; \quad \frac{\mathrm{d}N}{\mathrm{d}t} = J_{\mathrm{N}} - J_{\mathrm{c}}, \tag{48}$$

where $S_i^{\mathrm{l}\to v} = -S_i^{\mathrm{nuc}} + S_i^{\mathrm{e-c}}$ with

$$S_i^{\mathrm{nuc}} = 2 J_{\mathrm{N}} N_i m_i, \tag{49}$$

$$S_i^{\mathrm{e-c}} = 2\pi D_i \overline{d} \rho Y_i^{\mathrm{s}} f(\overline{d}, \lambda)\Big(E_i - \frac{S_i}{W_i}\Big) N, \tag{50}$$

and the nucleation and coalescence rates are given by

$$J_{\mathrm{N}} = R_{\mathrm{av}} Z c_{\mathrm{eq}}; \quad J_{\mathrm{c}} = \overline{K} N^2. \tag{51}$$

This model system captures the main nucleation dynamics and will be specified for the simulation of the dynamics of a supercritical alcohol mixture. Nucleation is induced in this case by external cooling at temperature drop $\Delta T = T_1 - T_2$ ($T_{\mathrm{ref}} < T_2 < T_1$) for which we impose an external temperature given by a linear ramp

$$T = \begin{cases} T_1; & 0 \le t \le t_1, \\ T_1 \frac{t_2 - t}{t_2 - t_1} + T_2 \frac{t - t_1}{t_2 - t_1}; & t_1 \le t \le t_2, \\ T_2; & t_2 \le t. \end{cases} \tag{52}$$

In order to start the simulation of a cooling experiment, an initial condition needs to be specified. Taking temperature $T = T_1$ as initial condition we may specify the mole fractions of the different species based on Dalton's law. In fact, if the individual species have saturations (or 'activities') collected in a vector $\mathbf{S} = [S_2, \ldots, S_n]$ then the mole fractions of the alcohol components at system pressure p follow from $\mathbf{X}_0^{\mathrm{alc}} = (p_{\mathrm{s}}(T_1)/p)\mathbf{S}$. To complete the mole fractions and represent the ambient air, we use normalization of $\mathbf{X}_0$ such that $\mathbf{X}_0 = [1 - \sum_{i=2}^{n} X_{0,i}^{\mathrm{alc}}, X_{0,2}^{\mathrm{alc}}, X_{0,3}^{\mathrm{alc}}, \ldots, X_{0,n}^{\mathrm{alc}}]$. The corresponding mass fractions are found from

$$Y_{0,i} = \frac{m_i X_{0,i}}{\sum_{j=1}^{n} m_j X_{0,j}}. \tag{53}$$

The initial condition is completed by assuming that at $t = 0$ there are no aerosol droplets and all components are in the vapor state, i.e., $Z_{i,0} = 0$ and $N_0 = 0$.

The composition of the critical cluster is a key element in the description of a nucleation burst. In the next section, we turn to this problem and illustrate the effects of changing the saturation of the various components on the composition of the cluster.

3 Numerical methods for efficient time-stepping and critical cluster computations

In this section, we present and illustrate the method used to compute the critical cluster composition (Sect. 3.1) and discuss the adaptive time-stepping method used for efficient simulation of the multiscale problem that includes a rapid nucleation burst next to evaporation and condensation, as well as much slower coalescence effects (Sect. 3.2).

3.1 Critical cluster composition

The composition of the critical cluster can be computed following the discussion presented in Sect. 2.2. The mole fractions of the various species in the critical clusters $\{w_i\}$ are given in terms of saturation S_i and partial molar volume v_i by

$$w_i = S_i \exp(-\alpha v_i), \tag{54}$$

subject to the condition that

$$f(\alpha) \equiv \left(\sum_{i=1}^{n} S_i \exp(-\alpha v_i) \right) - 1 = 0, \tag{55}$$

for the parameter α. This condition guarantees that $\{w_i\}$ is a proper partition of unity, and requires a root of f to be found.

For technical convenience we rewrite (55) by introducing the dimensionless variable

$$\xi = \alpha v_1, \tag{56}$$

which has the benefit that it is expected to be of order unity, while α by itself is likely to be a very large reciprocal volume, to compensate for the very small numerical values of v_i. In addition, we use the dimensionless system parameters

$$\phi_i = \frac{v_i}{v_1}; \quad i = 1, \ldots, n, \tag{57}$$

which represent the ratios between partial molar volumes. This notation allows to write

$$f(\xi) = \left(\sum_{i=1}^{n} S_i \exp(-\xi \phi_i) \right) - 1 = 0. \tag{58}$$

An effective algorithm for determining ξ from (58) is Newton iteration for which we construct a sequence

$$\xi_{k+1} = \xi_k - \frac{f(\xi_k)}{f'(\xi_k)}; \quad k \geq 0, \tag{59}$$

in which, explicitly

$$f'(\xi) = -\sum_{i=1}^{n} \phi_i S_i \exp(-\xi \phi_i). \tag{60}$$

The iteration can be continued until an appropriate level of convergence is achieved, e.g., when $|\xi_{k+1} - \xi_k| < \varepsilon$, for some appropriate tolerance $\varepsilon > 0$. Since $|w_i| < 1$, $|v_i| < 1$ for all species i, and $\sum_{i=1}^{n} w_i = 1$, the Newton iteration is converging as it can be shown that $f'(\alpha) < 1$ for $f'(\alpha) = -\sum_{i=1}^{n} v_i w_i$, which is equivalent to the Eq. (60). To start the process a suitable initial condition should be selected. For a single-species system we may write

$$f(\xi) = S_1 \exp(-\xi) - 1 = 0, \tag{61}$$

which can be explicitly solved to yield

$$\xi = -\ln(S_1^{-1}). \tag{62}$$

This can be taken to start the iteration process for multispecies systems and is expected to be not too far from the actual value in cases in which one of the species is dominant in the nucleation process. We may generalize this initial condition to

$$\xi = -\max_{i=1,\ldots,n} \left(\ln(S_i^{-1}) \right), \tag{63}$$

to cover cases where the dominant species is not the species labeled number one.

We illustrate the performance of the Newton iteration to determine the composition of the critical cluster. We construct some characteristic cases that show the general change in composition in case saturations and molar volume ratios is systematically varied. First, we turn attention to a two-species situation in which one species dominates in terms of saturation, taking $S_1 = 1 + \beta$ and $S_2 = 1 - \beta$ with $0 < \beta < 1$. We consider these two species to have molar volumes given by $\phi_2 = \gamma$. In Fig. 1, we show the dependence of $\{w_1, w_2\}$ on the parameter characterizing the saturation dominance β, at a number of molar volume ratios γ. The Newton iteration was found to converge to machine accuracy within 5-8 iterations for this case, leading to only a very small computational cost

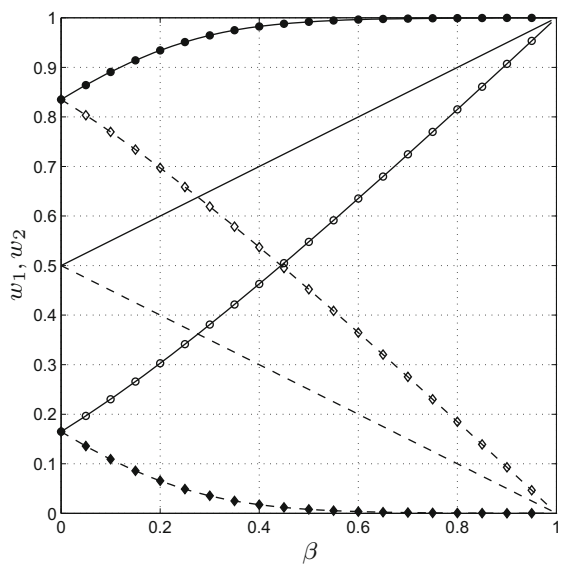

Fig. 1 Variation of composition of the critical cluster for a two-species mixture, showing the mole fractions of the two components as function of β characterizing the saturation $S_1 = 1 + \beta$ and $S_2 = 1 - \beta$. We show results at different molar volume ratios $\gamma = v_2/v_1$. Results for the mole fraction w_1 are shown with *solid lines* and/or *circles* (*open circle*, *filled circle*), while the mole fraction w_2 is shown using *dashed lines* and/or *diamonds* (*open diamond*, *filled diamond*). In addition, markers label the following: $\gamma = 10$ (solid marker: *filled circle*, *filled diamond*), $\gamma = 1$ (no marker), $\gamma = 0.1$ (open marker: *open circle*, *open diamond*)

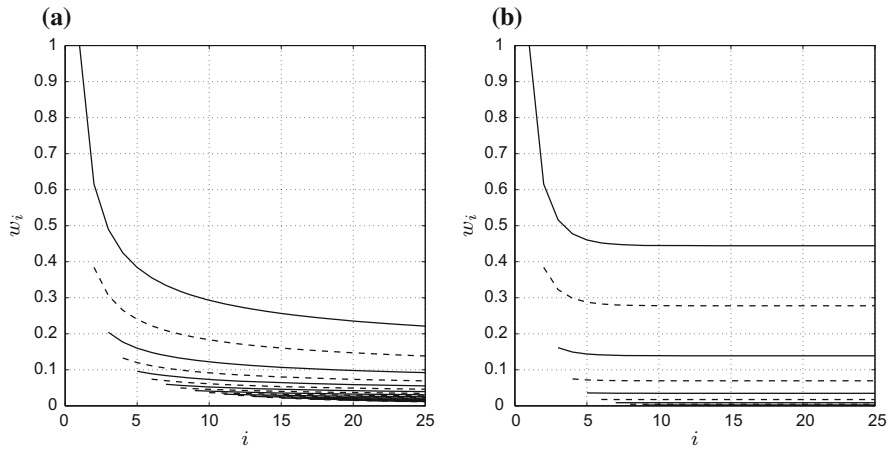

Fig. 2 Mole fractions $\{w_i\}$ in the critical cluster as a function of the number of species included in the gas phase. From *top* to *bottom* w_i is shown for $i = 2j - 1$ (*solid*) and $i = 2j$ (*dashed*) for $j = 1, 2, \ldots$. In **a** one species is dominant with $S_1 = 2$ and the saturation of the sub-dominant species is given by $S_i = \beta 2^{-i}$ with $\beta = 5$. In **b** the saturation of the sub-dominant species is given by $S_i = \beta/(2i)$, for $i = 2, \ldots$. All molar volumes are considered equal, i.e., $\phi_i = 1$

for determining the constitution of the critical cluster. In case $\gamma = 1$ we observe that as $\beta \to 0$, both species are present with equal mole fraction $w_1 = w_2 \to 1/2$, as was to be expected. Increasing β in this case, i.e., increasing the saturation of component '1', $S_1 > 1 > S_2$, leads to a linear increase (decrease) of the mole fraction w_1 (w_2) with β. As $\beta \to 1$ component '2' becomes negligible in the critical cluster and we enter the single-species limit with clusters consisting entirely of component '1'. Changing the ratio of the molar volume γ has a marked effect on the composition. We notice that an increase in $\gamma > 1$, i.e., in case the molar volume of component '2' is larger than that of component '1,' further increases the presence of the dominant species in the critical cluster. The reverse arises in case $\gamma < 1$ and we observe that even though $S_1 > S_2$ the small molar volume of component '2' favors this component over '1' in the critical cluster.

The Newton iteration can also be adopted to solve the critical cluster equation in cases in which many species make up the gas phase. There are many possible situations that one can use to illustrate the current formulation. We restrict ourselves to a situation in which $\phi_i = 1$, denoting systems for which the molar volume v_i does not depend on the index. We consider two situations in which species '1' is dominant and supersaturated, e.g., $S_1 = 2$ and consider sub-dominant species with (a) $S_i = \beta 2^{-i}$ and (b) $S_i = \beta/(2i)$ for $i \geq 2$, with $\beta = 5$. In Fig. 2, we show the mole fractions $\{w_i\}$ for these two situations as function of the number of species included in the formulation. In both situations, the Newton iteration was found to converge very rapidly. We notice that in case (a), the sub-dominant contributions for $n \gtrsim 10$ can effectively be neglected and a good representation of the critical cluster appears not to require more species in the model. In case (b), the sub-dominant species do not reduce in saturation as rapidly and the composition of the critical cluster is much richer and many more species need to be included before an accurate prediction of the composition can be achieved.

The key step of computing the composition of the critical cluster on the basis of Newton iteration was found to be possible even for large numbers of species. This makes it possible to study the extended classical nucleation theory for many species in a dynamic setting, including also evolution of the nucleating aerosol due to evaporation and condensation.

3.2 Adaptive time-stepping for rapid nucleation bursts and slow coalescence

In order to efficiently simulate the evolution of the aerosol subject to rapid nucleation during the initial stages as well as to the long term much slower coalescence, it is natural to adopt a time-stepping method that adapts to the

actual instantaneous time scale. We maintain control over the time-accuracy by keeping the size of the time-step appropriately small during the rapid nucleation stages, while increasing the size of the time-step in case the dynamics so allows.

The structure of the adaptive time-integration method allows to increase the size of the time-step as well as to decrease it. Specifically, at some point during the time integration we have obtained the numerical solution $u(t_n)$ at time t_n and the time-step has size δt. We then proceed as follows:

- Using the basic propagation algorithm for performing an explicit time-step we may compute the numerical solution in the next two instants of time, i.e., $u_{\delta t}(t_{n+1})$ and $u_{\delta t}(t_{n+2})$ with $t_{n+1} = t_n + \delta t$ and $t_{n+2} = t_n + 2\delta t$. Here, we added the subscript δt to indicate that the numerical solution was obtained using time-step δt.
- The solution at t_{n+2} may also be approximated using one time-step of size $2\delta t$, denoted by $u_{2\delta t}(t_{n+2})$.
- Likewise, we may approximate the solution at t_{n+2} by taking four time-steps of size $\delta t/2$, denoted by $u_{\delta t/2}(t_{n+2})$.
- We determine the relative differences $\epsilon_{2\delta t} = \|u_{2\delta t}(t_{n+2}) - u_{\delta t}(t_{n+2})\|/\|u(0)\|$ and $\epsilon_{\delta t/2} = \|u_{\delta t/2}(t_{n+2}) - u_{\delta t}(t_{n+2})\|/\|u(0)\|$. Specifically, we concentrate on the ethanol component in our model system to monitor the accuracy of the time integration, i.e., we take $u = Y_1$ in this paper.

Based on the relative differences $\epsilon_{2\delta t}$ and $\epsilon_{\delta t/2}$, we may proceed with updating the size of the time-step. If $\epsilon_{2\delta t} < \epsilon_{\text{tol}}$ then the size of the time-step is increased by a factor $a > 1$, i.e., $\delta t \to a\delta t$. Conversely, if $\epsilon_{\delta t/2} > \epsilon_{\text{tol}}$ then the time-step is decreased by the same factor, i.e., $\delta t \to \delta t/a$. Finally, if $\epsilon_{2\delta t} > \epsilon_{\text{tol}}$ and $\epsilon_{\delta t/2} < \epsilon_{\text{tol}}$ then the time-step is left unchanged.

We adopted Euler forward time-stepping as basic propagation algorithm in the simulations. Obviously, this is not a strict requirement and the same general approach can be combined with other, higher-order explicit time-stepping methods. In the simulations we use a time-step stretching factor of $a = 1.2$ when increasing or decreasing the time-step size. We limit the time-step to $\delta t_{\max}$ such that the solution remains stable and time-accurate even for the slowest time scales. The initial size of the time-step is taken sufficiently small to capture the brief nucleation burst that occurs during the sharp cooling ramp. Finally, the value of the tolerance needs to be specified to control the adaptation of the time-step. How precisely to specify these numerical parameters is a matter of some experimentation in actual examples. We turn to the evolution of the aerosol emanating from a mixture of alcohol vapors in the next section and illustrate the specification of the numerical control parameters.

4 Dynamics of aerosol formation from rapidly cooled alcohol vapors

In this section, we first specify the computational model with which the aerosol evolution under rapid cooling of a mixture of alcohol vapors can be simulated; we will address the connection with the Becker–Döring theory by exploiting the detailed numerical solution as presented by Van Putten et al. [2], and quantify the relevance of the Wilemski normalization for this situation (Sect. 4.1). The resulting computational model is subsequently applied to analyze the aerosol dynamics of the multispecies alcohol vapors under different cooling rates and temperature levels, focusing on droplet sizes and their number density (Sect. 4.2).

4.1 Numerical model for aerosol formation from alcohol vapors

The formation of an aerosol from a multispecies alcohol vapor mixture due to rapid cooling can be simulated with the extended classical nucleation theory as presented in Sect. 2. Here, we focus on the nucleation and subsequent evaporation/condensation and coalescence in the absence of fluid motion, i.e., we concentrate on the model system (48). We focus on the mixture of alcohol vapors as this is a well-established model system that was considered by various sources in literature [5]. It serves to illustrate the capability of the approach and can be extended to other applications by specifying the appropriate thermo-physical properties of the constituents.

A key element in the aerosol formation is the nucleation rate J_{N}. As discussed earlier, the normalization of the equilibrium concentration of critical clusters c_{eq} is subject to discussion in literature. In order to find out the accuracy

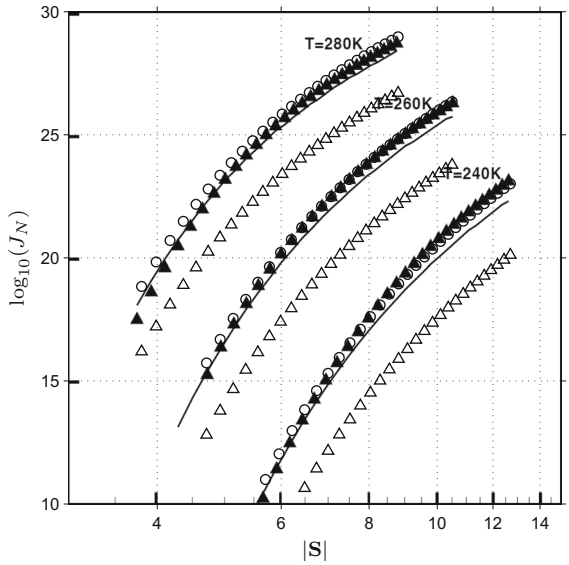

Fig. 3 Comparison of nucleation rate J_N (in $m^{-3}s^{-1}$) as obtained by the full Becker–Döring theory (*solid triangles*), steady-state classical nucleation theory based on Reiss [24] as used in [5] (*solid line*), extended classical nucleation theory following Stauffer et al. [25], with normalization (17) (*open triangles*), and with self-consistent normalization (19) (*open circles*). Results are shown at three different temperature levels, i.e., 240, 260, and 280 K, as indicated in the plot

of the proposed models, we compare (17) and (19) with the reference Becker–Döring result for a ternary system of ethanol, propanol, and hexanol in air, as obtained in [2]. In Fig. 3, we show the predicted J_N at three different temperatures. To obtain this result, we closely follow [5] and consider a system at pressure $p = 66.76$ kPa. We vary the saturation of the species while keeping their ratios unchanged, i.e., $S_{\text{propanol}}/S_{\text{ethanol}}$ and $S_{\text{hexanol}}/S_{\text{ethanol}}$ are kept constant at 1.2 and 4, respectively. The mass fractions follow from (53), using Dalton's law. We plot J_N as a function of $|\mathbf{S}| = \sqrt{S^2_{\text{ethanol}} + S^2_{\text{propanol}} + S^2_{\text{hexanol}}}$.

All models included display quite similar trends but there is a significant underestimation of J_N in case the normalization as presented in Eq. (17) is adopted. As the classical nucleation approach is not a 'first-principle' theory but largely a phenomenological model, various corrections/normalizations are applied to it that better suit the validation purposes for certain chemical compounds or that are mathematically appealing in an asymptotic limit. For example, the underestimation of two to three orders of magnitude of nucleation rate is almost completely corrected when Eq. (19) is adopted. The corresponding predictions correspond quite closely with the numerical solution to the full Becker–Döring theory as obtained in [2]. The current extended classical nucleation theory with normalization as in Eq. (19) yields an accurate agreement with the full Becker–Döring approach, at very low computational cost in contrast to the full n-component Becker–Döring (NBD) equations [5], for which comparative results were obtained at a substantial computational cost using multigrid methods. We notice that the steady-state classical nucleation theory based on Reiss [24] almost coincides with our prediction for J_N, which is based on earlier work of Stauffer et al. [25], establishing that both the Reiss and Stauffer approaches yield quite similar results for J_N.

We next turn to the actual simulation of a reference cooling experiment and specify in further detail the numerical parameters as required in the adaptive time-stepping method. We consider the system to be initially at a temperature $T_1 = 275$ K and allow it to cool to $T_2 = 200$ K in a time interval of 0.01 s, choosing $t_2 = 0.01$ s and $t_1 = 0$ s. The nucleation burst and subsequent condensation and afterwards coalescence are simulated until $t = 0.05$ s, at which time the dominant remaining mechanism is that of slow coalescence. In order to track the rapid initial behavior and also integrate for sufficiently long times, we put $\delta t_0 = (t_2 - t_1)/10^{n_{\delta t}}$ and limit the maximal time- step to $\delta t_{\max} = 10^{-4} - 10^{-3}$, which was found to be close to the stability time-step in the selected settings. The tolerance ϵ_{tol} controls the adaptation of the time-step size. We put it to $\epsilon_{\text{tol}} = 10^{-n_{\text{tol}}}$ and investigate the role of $n_{\delta t}$ and n_{tol} in relation to the accuracy of the simulations.

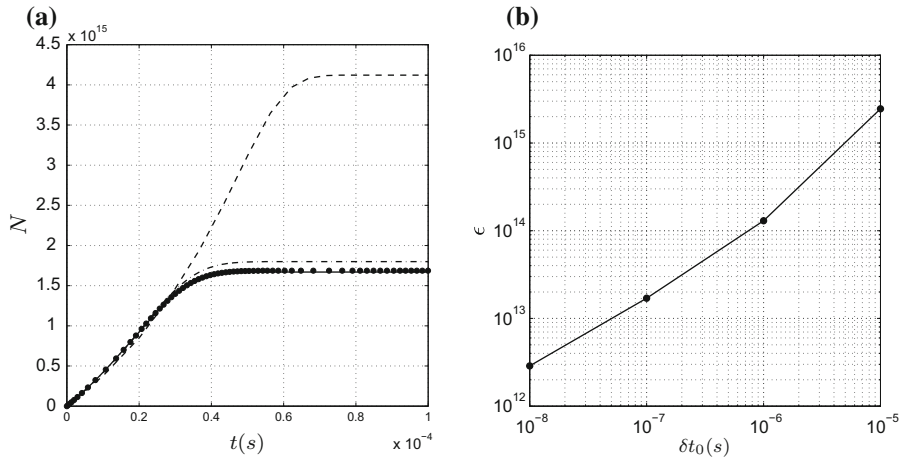

Fig. 4 Dependence of the number density N (per m^3) of aerosol droplets on time-integration step: in **a** we show $N(t)$ for the reference case when changing the initial time-step size δt_0: 10^{-5} (*dash*), 10^{-6} (*dash-dot*), 10^{-7} (*dot*), 10^{-10} (*solid*), and in **b** the behavior of the error in the final number density ϵ with decreasing δt_0 is shown. We set the adaptation threshold $\epsilon_{\text{tol}} = 10^{-5}$ and use a time-step stretching factor $a = 1.2$

In Fig. 4a, we show the evolution of the number density N during the nucleation burst. The initial time-step was varied from $\delta t_0 = 10^{-10}$ s to $\delta t_0 = 10^{-5}$ s. We observe a rapid increase in the number of droplets in the system as a result of the very strong nucleation burst in the selected reference case. This behavior is well captured by the adaptive time-stepping method in case the size of the initial time-step is sufficiently small. The convergence of this numerical process is shown in Fig. 4b. Here, we show the difference ϵ between N at $t = 10^{-4}$ s as obtained at the indicated initial time-step size and the highly resolved case at $\delta t_0 = 10^{-10}$, i.e., $\epsilon = |N(\widetilde{t}; \delta t_0) - N(\widetilde{t}, 10^{-10})|$ where the monitoring moment is chosen in the asymptotic range at $\widetilde{t} = 10^{-4}$ s. This clearly illustrates the first-order convergence of the global error. Moreover, it establishes the relevance of capturing the very early stages of the nucleation burst with high precision, in order to compute the total number density of aerosol droplets that results. From these simulations it appears safe to set $\delta t_0 = 10^{-10}$ s as this is certainly small enough to capture the nucleation burst under the selected circumstances while not adding much to the overall simulation time in view of the geometric stretching of δt in the adaptation strategy.

In Fig. 5a, we present the dependence of the number density N on the adaptation threshold ϵ_{tol}. We observe a close agreement in capturing the initial transient up to $t \approx 2 \times 10^{-5}$ s as the time-step is still sufficiently small in this part of the evolution. As the nucleation burst draws to an end and the number density approaches its asymptotic value for $t \gtrsim 5 \times 10^{-5}$ s we notice still quite some dependency on the adaptive time-stepping strategy. The asymptotic value $N(\infty)$ is seen to vary about 3% when changing the threshold from $\epsilon_{\text{tol}} = 10^{-8}$ at which a 'converged' solution is attained to $\epsilon_{\text{tol}} = 10^{-5}$. The variation of the time-step in the course of a simulation is shown in Fig. 5b. We observe a distinctive rapid increase in δt during the very first part of the evolution. At all values of ϵ_{tol} the time-step simply increases according to the time-step stretching factor a that is adopted. Subsequently, the time-step displays a characteristic dependence on time, reflecting the passing of the strict nucleation burst and the transitioning to the phase influenced more by condensation. If $\epsilon_{\text{tol}} \lesssim 10^{-4}$ a striking similarity is observed in δt for all ϵ_{tol} in which δt varies roughly by a factor $10 - 50$ upon decreasing ϵ_{tol} from 10^{-4} to 10^{-8}. This increase in accuracy, however, comes at the same factor of $10-50$ increase in computational effort. Since the variation of N with, e.g., temperature level and/or cooling rate, is much more than a few percent, it is sufficient to require a 'fair' overall accuracy of better than, say, 5%, which implies to use $\epsilon_{\text{tol}} = 10^{-5}$ in the sequel. This also yields much more acceptable computing times than in case of requiring a fully time-step independent solution.

We complete the investigation of the time-stepping approach by considering the effect of the time-step stretching factor a. For that purpose we set $\epsilon_{\text{tol}} = 10^{-5}$ and use $\delta t_0 = 10^{-10}$ s. In Fig. 6a, we show the direct effect of the stretching a on the evolution of N. We observe that an increase in the stretching factor, i.e., adaptation leading to

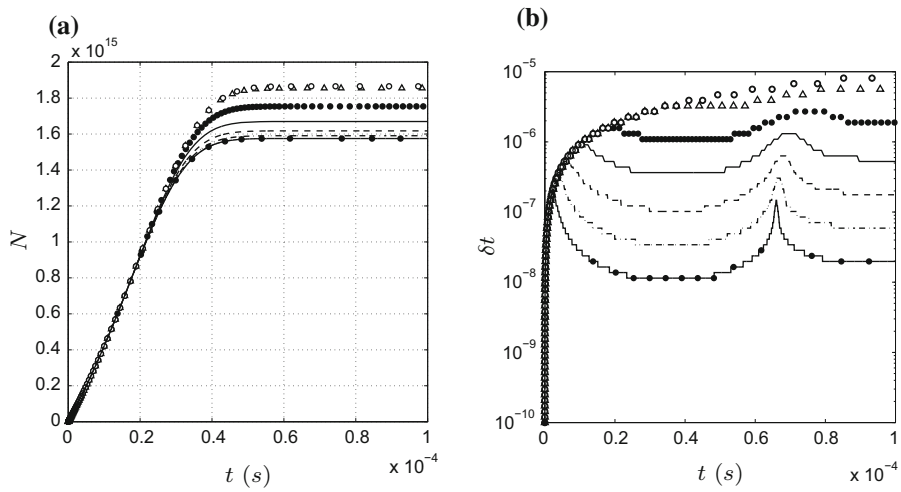

Fig. 5 Evolution of the number density N (per m^3) of aerosol droplets at various adaptation thresholds ϵ_{tol} (**a**) and variation of the time-step δt in the course of the nucleation and evaporation/condensation processes (**b**). Curves are labeled with the value of ϵ_{tol} as follows: *open circle* (10^{-2}), *open triangle* (10^{-3}), *dot* (*filled circle*) (10^{-4}), *solid* (10^{-5}), *dash* (10^{-6}), *dash-dot* (10^{-7}), and *solid with dot* (*filled circle*) (10^{-8}). We set $\delta t_0 = 10^{-10}$ in these simulations and use a time-step stretching factor $a = 1.2$

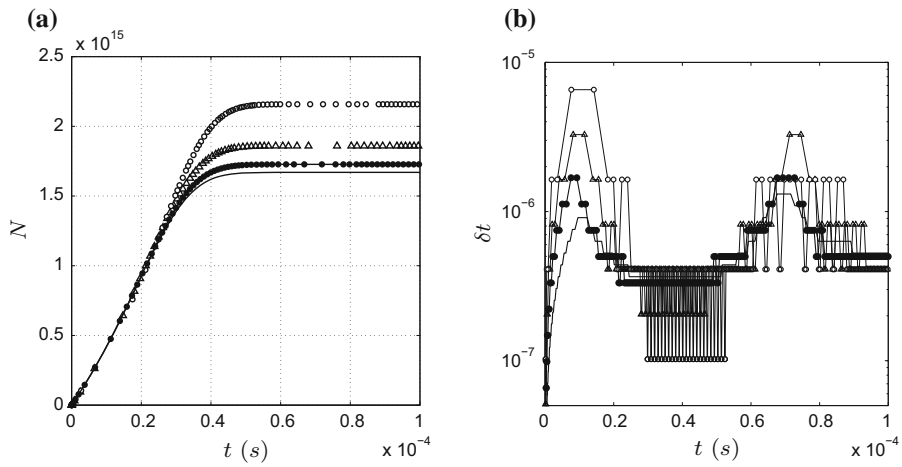

Fig. 6 Evolution of the number density N (per m^3) of aerosol droplets at various time-stretch factors (**a**) and variation of the time-step δt in the course of the nucleation and evaporation/condensation processes (**b**). Curves are labeled with the value of a as follows: *circle* ∘ ($a = 4$), *triangle open triangle* ($a = 2$), *solid with dot filled circle* ($a = 1.5$), *solid* ($a = 1.2$). We set $\delta t_0 = 10^{-10}$ in these simulations and use $\epsilon_{\text{tol}} = 10^{-5}$

very rapid growth and reduction of the time-step, yields an overestimation of the asymptotic value of N by 35% in case $a = 4$. This is reminiscent of the effect of a relatively high value of ϵ_{tol} as shown in Fig. 5. The time-step variations in the course of time are shown in Fig. 6b. We observe that a large value of a not always implies highest δt. Rather, the variations are highest as is the increase in δt initially. The algorithm can also yield rapidly oscillating behavior in δt, as observed in case $a = 2$. Although this is not diminishing the overall accuracy in case the Euler forward scheme is used, it could lead to unwanted numerical errors when higher-order methods would be adopted. Adhering to an overall accuracy level in the asymptotic value of N of better than about 5% we select as stretching factor $a = 1.2$ in the sequel.

After these exploratory investigations of the numerical treatment of the nucleation burst, we proceed by investigating the physical implications of changing the temperature level and the cooling rate on the vapor and liquid phases as well as on the aerosol droplet properties such as number density and size.

4.2 Aerosol dynamics in multispecies alcohol vapor mixtures

In order to illustrate the capability of the proposed model to deal with nucleation, condensation, and coalescence of multiple species under different process conditions, we collect several characteristic illustrations in this section. First the effect of the overall temperature level is investigated, keeping the cooling rate fixed. Subsequently, the effect of cooling rate on the aerosol size distribution and chemical composition of the droplets is considered. Finally, we present an example in which we compare aerosol properties arising in alcohol mixtures containing different numbers of species.

Next to the system pressure, the temperature and the rate of cooling are decisive of the response of the system. Throughout, the system pressure is kept constant at 66.75 kPa. We are interested in the effect of rapid cooling of a vapor mixture, leading to supersaturation and the formation of an aerosol following a rapid nucleation burst. For this purpose, we consider a reference case in which we decrease the temperature by $\Delta T = 75$ K within 0.01 s. The properties of an aerosol that forms strongly depend on the thermodynamic state and properties of the system. For example, results obtained at various cooling rates show a significantly different temporal behavior in formation of the liquid phase (droplets) due to nonlinearity of the nucleation process. Figures are presented in a way that we feel gives the best illustration of the nonlinear behavior and shows the sensitivity to the chosen conditions.

In the first set of numerical experiments, we consider the effect of changing the overall temperature level for the ternary alcohol mixture, which was used in [2] with saturations given by $\mathbf{S} = [1, 1.2, 0, 0, 4]$ indicating the presence of ethanol, propanol, and hexanol, respectively, in our model system. In Fig. 7, we show the evolution of the number density of droplets and the ethanol vapor concentration. The number concentration of droplets is seen to undergo rapid algebraic growth for short times on the order of 10^{-4} to 10^{-3} s after which a strong short-lived increase in this growth is observed, which we identify with the nucleation burst. This increased growth rate in N is strongest in case the initial temperature is sufficiently low. Subsequently, the number density settles down to a characteristic value, marking the end of the nucleation burst around 10^{-2} s. The dependence on the temperature level is striking. A reduction in the temperature leads to a strong reduction in the initial number of droplets in the system, before the dominant burst. The behavior of the vapors in the system shown in Fig. 7b displays a similar rapid decrease leading to almost complete depletion of the ethanol content around $t = 10^{-2}$ s. We notice that at lower initial temperatures the vapor initially does not decrease significantly, but a rapid decrease takes place as the nucleation burst sets in from the moment the vapor mixture becomes supersaturated. We observe that at $T_1 = 275$ K the nucleation starts directly from $t = 0$, while at lower initial temperatures, leading also to lower initial vapor concentrations of ethanol etc., further cooling is needed to generate the triggering supersaturated condition. This behavior is also clearly expressed in the behavior of propanol and hexanol in Fig. 7c and d, respectively, albeit at much lower concentrations and even faster time scales.

The approach developed in this paper can also be adopted to investigate the effect of the cooling rate on the developing multispecies aerosol. For this purpose, we set the initial temperature to $T_1 = 255K$ and traverse the temperature drop within a time interval of 0.02, 0.04, 0.08, and 0.16 seconds. We observe in Fig. 8a that, with decreasing cooling rate the number concentration of aerosol droplets also strongly decreases. Simultaneously, we notice that the onset of nucleation is also delayed somewhat with decreasing cooling rate. This behavior is similarly observed in the evolution of the vapor concentrations, e.g., shown by the decay of ethanol in Fig. 8b, in which a slightly delayed nucleation can be observed as well at lower cooling rates. Moreover, we notice that decreasing the cooling rate leads to a slowing down of the consumption of the alcohol vapors in the aerosol formation. The total process appears to slow down proportionally to the size of the time interval during which the temperature drop takes place.

The total amount of vapor that is consumed during nucleation and subsequent condensation remains virtually identical—at lower cooling rate it only takes longer for the vapors to be transferred to the liquid droplets. Moreover, in the current setting we observe that virtually all vapor is consumed in the aerosol formation—only a small residual vapor concentration remains at the end of the cooling ramp. Combined with Fig. 8a showing a strong reduction of

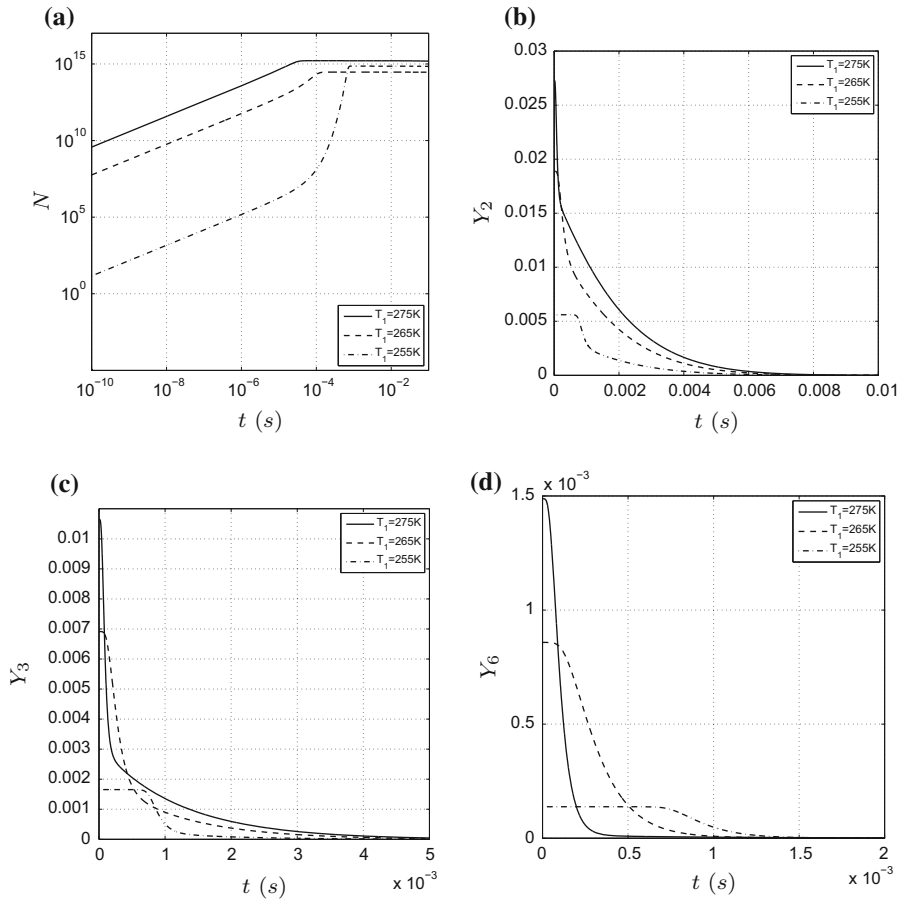

Fig. 7 Evolution of the number density N (per m^3) of aerosol droplets (**a**) and ethanol: Y_2 (**b**), propanol: Y_3 (**c**) and hexanol: Y_6 (**d**) vapor concentration showing the effect of changes in the system temperature. A cooling over $\Delta T = 75$ K in 0.01 s was adopted with starting temperature $T_1 = 275$ K (*solid*), $T_1 = 265$ K (*dash-dot*), and $T_1 = 255$ (*dash*)

N with decreasing cooling rate, this implies that fewer but larger droplets are being formed at lower cooling rates. In order to quantify this we compute the evolution of the droplet size d_{m} as defined in (27) in time. This is shown in Fig. 9. We observe a slower rate at which N grows initially. More striking is the final size the aerosol droplets reach asymptotically. We notice a nearly six-fold increase when the cooling rate is reduced by a factor 16 in this example. Hence, careful control of the cooling rate is a very sensitive measure for managing the ultimate size of the droplets that are being formed.

As a further illustration of the extended classical nucleation approach we consider an example of a composite system containing up to five alcohols in air. We compare the aerosol formation process as well as changes in size and composition of the aerosol droplets. In many applications involving various species, several of the species are only 'residual', i.e., these species represent only a small fraction of the total mass in the system. In order to mimic this situation of dominant species next to additional 'residual' species we consider a saturation vector $\mathbf{S} = [1, 1/2, 1/4, 1/8, 1/16]$ for the five alcohols ethanol, propanol, butanol, pentanol, and hexanol respectively. In the sequel we adopt a temperature drop of $\Delta T = 75$ K in 0.02 s, starting from an initial temperature of 275 K. Of course, the selection of this saturation vector is for illustration purposes only, other situations may apply in specific applications. However, once the thermo-physical characterization of the constituents is available, the present method can be applied to predict the aerosol formation.

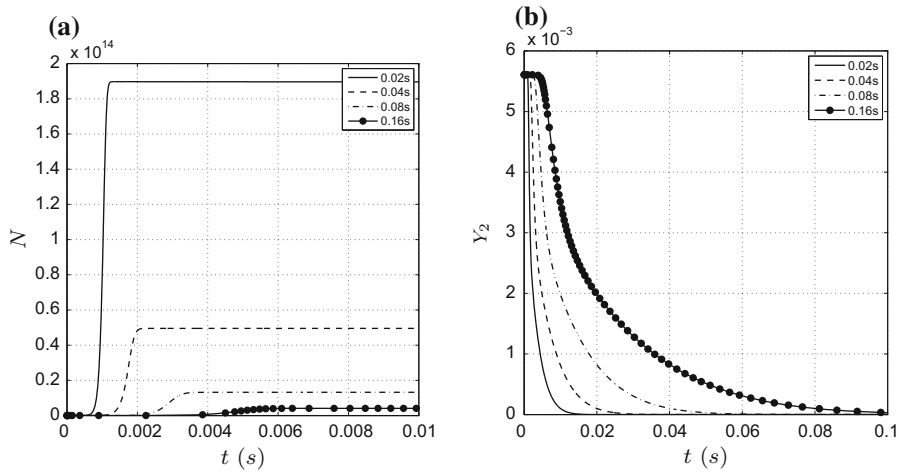

Fig. 8 Evolution of the number density N (per m^3) of aerosol droplets (**a**) and ethanol: Y_2 vapor concentration (**b**) showing the effect of changes in the temperature cooling rate. Cooling by $\Delta T = 75$ K during 0.02 s (*solid*), 0.04 s (*dash*), 0.08 s (*dash-dot*), and 0.16 s (*solid with dot filled circle*). The initial temperature $T_1 = 255$ K

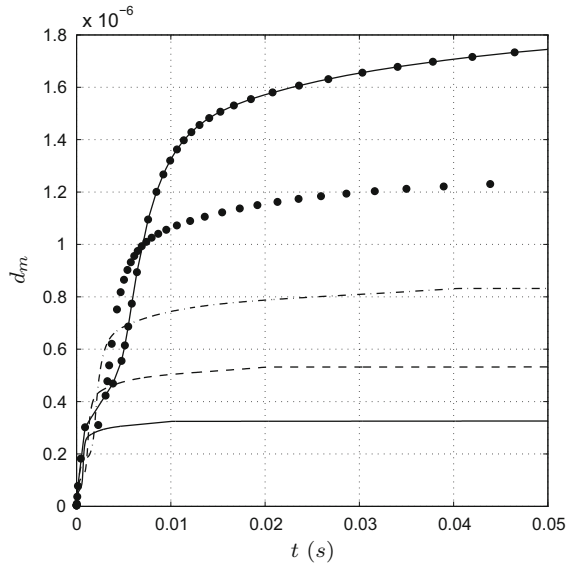

Fig. 9 Evolution of the size d_{m} (in m) of the droplets showing the effect of changes in the temperature cooling rate. Cooling by $\Delta T = 75$ K during 0.01 s (*solid*), 0.02 s (*dash*), 0.04 s (*dash-dot*), 0.08 s (*dot filled circle*), and 0.16 s (*solid with dot filled circle*). The initial temperature $T_1 = 255$ K

In Fig. 10a, the transfer of the various vapors to their liquid phase is illustrated in case all five alcohols are present in the mixture. We observe a somewhat similar dependence on time for all vapor concentrations. In the selected nucleation setting, there is a clear phase of about 0.002 s in which the mixture is not undergoing nucleation yet. After this a short period of rapid vapor consumption is observed in which all Y_i show an approximately exponential decay. This lasts for about 0.001 s for ethanol to about 0.004 s for hexanol. Subsequently a slower, also approximately exponential decay sets in until almost full depletion of all vapors around $t = 0.02$ s. The dependence of the vapor consumption on the constitution of the mixture is illustrated in Fig. 10b in terms of the evolution of the dominant ethanol concentration. We observe that removal of the 'higher alcohols' leads to a further delay of the onset of nucleation, from the mentioned 0.002 s in the full mixture up to about 0.004 s in case of pure ethanol. The decay rate following the onset of nucleation is largely insensitive to the constitution of the mixture, and after about 0.007 s all decay curves are seen to merge and continue independently of the initial differences in the mixture.

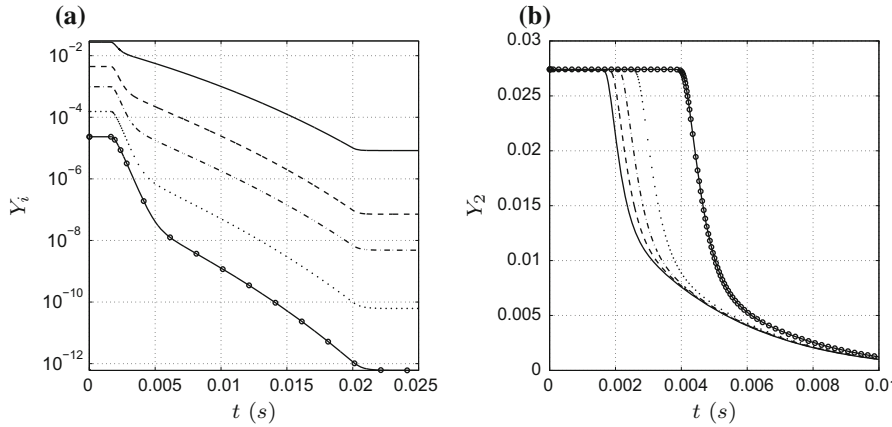

Fig. 10 Evolution of vapor fractions showing the individual species in case of five alcohols (**a**) with ethanol (*solid*), (*dash*), (*dash-dot*), (*dot*), (*solid and dot filled circle*), and the effect of removing 'residual' species on the ethanol concentration (**b**). Lines are labeled according to the saturation vector $\mathbf{S} = [1, 1/2, 1/4, 1/8, 1/16]$ (*solid*), $\mathbf{S} = [1, 1/2, 1/4, 1/8, 0]$ (*dash*), $\mathbf{S} = [1, 1/2, 1/4, 0, 0]$ (*dash-dot*), $\mathbf{S} = [1, 1/2, 0, 0, 0]$ (*dot filled circle*), $\mathbf{S} = [1, 0, 0, 0, 0]$ (*solid and dot filled circle*)

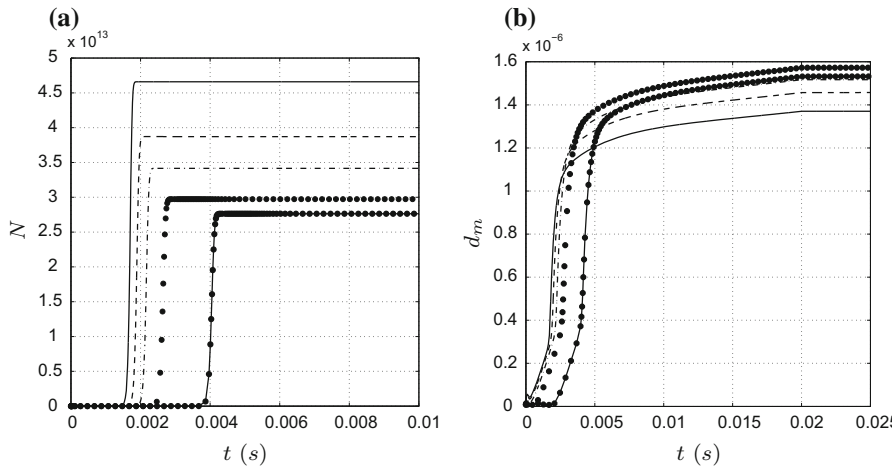

Fig. 11 Evolution of the number concentration (**a**) and droplet size (**a**) for increasing number of contributing species according to the saturation vector $\mathbf{S} = [1, 1/2, 1/4, 1/8, 1/16]$ (*solid*), $\mathbf{S} = [1, 1/2, 1/4, 1/8, 0]$ (*dash*), $\mathbf{S} = [1, 1/2, 1/4, 0, 0]$ (*dash-dot*), $\mathbf{S} = [1, 1/2, 0, 0, 0]$ (*dot filled circle*), $\mathbf{S} = [1, 0, 0, 0, 0]$ (*solid and dot filled circle*)

The consequences of the mixture composition on the number concentration and size of the developing aerosol are illustrated in Fig. 11. The asymptotic number concentration in Fig. 11a is seen to decrease by up to about 1/3 by simplification of the mixture. This has also consequences for the size of the developing aerosol droplets. As may be observed in Fig. 11b, simplification of the mixture leads to slightly delayed nucleation and smaller droplets initially, while asymptotically the droplet size is seen to be higher for the simplified mixtures.

5 Concluding remarks

The problem of multi-component nucleation was formulated in terms of an Euler–Euler model with continuous velocity, temperature, and components fields, both for the vapor and the liquid phases. In the classical multi-component approach as provided by the Becker–Döring theory [1], it is challenging to treat systems with large numbers of components. The current state of the art [5] is limited to modest numbers of components. Recent model

studies discussed systems with up to five components [3,5]. Experimentally, binary and ternary species nucleation is a challenging topic of ongoing investigations. We addressed the fully coupled classical nucleation theory as put forward in [3,4] and developed a computational model that is capable of treating systems of considerably higher complexity being aware of the limitations concerning predictions coming from the classical nucleation theory. The current method can be used to treat systems with many components, as illustrated by the evaluation of the multispecies nucleation rate J_N and the characteristics of the critical cluster in case up to 25 species were incorporated.

No principal nor computational reason appears not to include more complex vapor mixtures—application to environmental aerosols and to aerosols stemming from the processing of biomass and food products come within reach as soon as the thermo-physical basic information of the individual species is available. Nucleation of multispecies gas mixtures from oversaturated vapors is a very challenging topic. Experimental results display a wide range of prediction. Moreover, it is well known that the introduction of certain additives/traces may significantly alter the nucleation process [26]. Such aspects are not taken into account in classical nucleation theory. Hence, application of classical nucleation theory must be considered with care, particularly for systems with many species. Mathematically, our approach does not have limitations in the number of species as for example presented in [27] and certainly more sophisticated methods can be used for the time-stepping algorithms as it can be found in [28].

The level of complexity required to capture a certain fraction of the total mass of components in the droplets can be illustrated by considering the convergence of the critical cluster as function of the number of components retained in the model. Where one might be tempted to take a rather small number of components in the model in view of practical limitations, the extended classical nucleation approach allows to compute many species and identify the number $\widetilde{n}$ of components needed to describe the aerosol formation with sufficient accuracy. This is basic to developing coarsened descriptions of aerosol-forming vapor mixtures that include a very large number of species, e.g., in atmospheric conditions over urban areas or in consumption of smoking articles and tobacco-related research. The Newton iteration that was used to solve the mole fraction equation was found to converge to machine accuracy within 5–8 iterations. For a wide range of characteristic nucleation conditions, the convergence was found to be quite independent of the number of species that was included in the problem.

In order to capture the wide range of time scales in the system, a simple adaptive time-stepping method was developed and used in conjunction with Euler forward time integration. A range of 5–6 orders of magnitude between the size of the initial time-steps and time-steps that can be used after the nucleation burst, in case condensation and coalescence dominate, was found to be achievable, leading to a significant saving of computation time. Further improvements may be possible by combination of higher-order time-stepping and the inclusion of specific physical simplifications that provide accurate approximations during certain stages of the evolution, e.g., during the late stages of dominant condensation/coalescence, but also during the initial phase where nucleation characterizes the full response to the employed cooling.

The illustration of the effects of (a) temperature level, (b) cooling rate, and (c) mixture composition on the properties of the developing aerosol show that the extended classical nucleation approach adopted in this paper can be used effectively for spatially homogeneous systems. This capability will be integrated with laminar flow of the aerosol-forming species and hence constitute a comprehensive computational model with which physical experiments conducted in LFDC equipment can be simulated. This is subject of ongoing research and will provide a full comparison with experimental data, allowing a validation of the method.

Acknowledgements The research presented in this work was funded by Philip Morris Products S.A. (part of Philip Morris International group of companies).

References

1. Becker R, Döring W (1935) Kinetische Behandlung der Keimbildung in Übersättigten Dämpfen. Ann Phys 24:719
2. van Putten DS, Glazenborg S, Hagmeijer R, Venner C (2011) A multigrid method for N-component nucleation. J Chem Phys 135:014114
3. Arstila H, Korhonen P, Kulmala M (1999) Ternary Nucleation: kinetics and application to water-ammonia-hydrochloric acid system. J Aerosol Sci 30:131–138
4. Wilemski G (1984) Composition of the critical nucleus in multicomponent vapor nucleation. J. Chem. Phys. 80:1370–1372
5. van Putten DS (2011) Efficient methods for N-component condensation. Ph.D. dissertation. University of Twente, Enschede
6. Winkelmann C, Nordlund M, Kuczaj A, Stolz S, Geurts B (2014) Efficient second-order time-integration for single-species aerosol formation and evolution. Int J Numer Methods Fluids 74(5):313–334
7. Frederix E, Stanic M, Kuczaj A, Nordlund M, Geurts B (2015) Extension of the compressible PISO algorithm to single-species aerosol formation and transport. Int J Multiph Flows 74:184–194
8. Poling B, Prausnitz J, O'Connell J (2001) The properties of gases and liquids, 5th edn. McGraw-Hill, New York
9. Whitby E, McMurry P (1997) Modal aerosol dynamics modeling. Aerosol Sci Technol 27(6):673–688
10. Wölk J, Strey R (2001) Homogeneous Nucleation of H_2O and D_2O in comparison: the Isotope effect. J Phys Chem B 105(47):11683–11701
11. Bird R, Stewart W, Lightfoot E (1960) Transport phenomena. Wiley, New York
12. Fuller E, Ensley K, Giddings J (1969) Diffusion of halogenated hydrocarbons in helium. J Phys Chem 73:3679
13. Magnusson L, Koropchak J, Anisimov M, Poznjakovskiy V, de la Mora J (2003) Correlations for vapor nucleating critical embryo parameters. J Phys Chem Ref Data 32:1387
14. Wilemski G, Wyslouzil B (1995) Binary nucleation kinetics. I. Self-consistent size distribution. J Chem Phys 103:1127
15. Kashchiev D (2000) Nucleation: basic theory with applications. Elsevier Science, Butterworth-Heinemann
16. Slezov V (2009) Kinetics of first-order phase transitions. Wiley, Weinheim
17. Friedlander S (1977) Smoke, dust and haze. Wiley, New York
18. Wilck M, Stratmann F (1997) A 2-D multicomponent modal aerosol model and its application to laminar flow reactors. J Aerosol Sci 28:959–972
19. Sirignano W (1999) Fluid dynamics and transport of droplets and sprays. Cambridge University Press, Cambridge
20. Hinds W (1999) Aerosol technology. Wiley, New York
21. Lee K, Chen H (1984) Coagulation rate of polydisperse particles. Aerosol Sci Technol 3:327–334
22. Fuller E, Schettler P, Giddings J (1966) A new method for prediction of binary gas-phase diffusion coefficients. Ind Eng Chem 58(5):19–27
23. Giovangigli V (1990) Mass conservation and singular multicomponent diffusion algorithms. Impact Comput Sci Eng 2:73–97
24. Reiss H (1970) Treatment of droplike clusters by means of the classical phase integral in nucleation theory. J Stat Phys 2(1):83–104
25. Stauffer D, Kiang C, Ennington A, Patterson E, Puri O, Walker G, Wise J Jr (1972) Heterogeneous nucleation and Fisher's droplet picture. Phys Rev B 6:2780
26. Kirkby J et al (2011) Role of sulphuric acid, ammonia and galactic cosmic rays in atmospheric aerosol nucleation. Nature 476: 429–433
27. Nordlund M, Kuczaj A (2016) Modeling aerosol formation in an electronically heated tobacco product. In: ICAST 2016, 18th international conference on aerosol science and technology, Lisbon, Portugal
28. Hairer E, Wanner G (1996) Solving ordinary differential equations. Springer Series in Computational Mathematics